0026-895X/09/7506-1280–1286$20.00
MOLECULAR PHARMACOLOGY
Copyright © 2009 The American Society for Pharmacology and Experimental Therapeutics
Mol Pharmacol 75:1280–1286, 2009

Vol. 75, No. 6
56242/3479312
Printed in U.S.A.

ACCELERATED COMMUNICATION

Targeted Disruption of the Multidrug and Toxin Extrusion 1 (*Mate1*) Gene in Mice Reduces Renal Secretion of Metformin

Masahiro Tsuda, Tomohiro Terada, Tomoyuki Mizuno, Toshiya Katsura, Jin Shimakura, and Ken-ichi Inui

Department of Pharmacy, Kyoto University Hospital, Kyoto, Japan (M.T., T.T., T.M., T.K., K.I.); and Pharmacokinetics Research Laboratories, Dainippon Sumitomo Pharma Co., Ltd., Osaka, Japan (J.S.)

Received March 17, 2009; accepted March 30, 2009

ABSTRACT

Multidrug and toxin extrusion 1 (MATE1/SLC47A1) is important for excretion of organic cations in the kidney and liver, where it is located on the luminal side. Although its functional and regulatory characteristics have been clarified, its pharmacokinetic roles in vivo have yet to be elucidated. In the present study, to clarify the relevance of MATE1 in vivo, targeted disruption of the murine *Mate1* gene was carried out. The lack of Mate1 expression in the kidney and liver was confirmed by reverse transcription-polymerase chain reaction and Western blot analysis. The mRNA levels of other organic cation transporters such as Octs did not differ significantly between wild-type [*Mate1*(+/+)] and *Mate1* knockout [*Mate1*(−/−)] mice. It is noteworthy that the *Mate1*(−/−) mice were viable and fertile. Pharmacokinetic characterization was carried out using metformin, a typical substrate of MATE1. After a single intravenous administration of metformin (5 mg/kg), a 2-fold increase in the area under the blood concentration-time curve for 60 min (AUC_{0-60}) of metformin in *Mate1*(−/−) mice was observed. Urinary excretion of metformin for 60 min after the intravenous administration was significantly decreased in *Mate1*(−/−) mice compared with *Mate1*(+/+) mice. The renal clearance (CL_{ren}) and renal secretory clearance (CL_{sec}) of metformin in *Mate1*(−/−) mice were approximately 18 and 14% of those in *Mate1*(+/+) mice, respectively. This is the first report to demonstrate an essential role of MATE1 in systemic clearance of metformin.

The elimination of drugs and xenobiotics is one of the key roles of the kidney and liver. The elimination of cationic drugs is mediated by a variety of organic cation transporters belonging to the SLC22 and SLC47 families, primarily expressed in the kidney and liver. The SLC22 family contains three subtypes of membrane potential-dependent organic cation transporters [OCT1 (SLC22A1), OCT2 (SLC22A2), and OCT3 (SLC22A3)] and two subtypes of the organic cation/carnitine transporters [OCTN1 (SLC22A4) and OCTN2 (SLC22A5)] (Inui et al., 2000; Koepsell et al., 2007). Human OCT1 and OCT2 are highly expressed in the basolateral membranes of the liver and kidney, respectively, and contribute to the uptake of cationic drugs from blood into the cell. Human OCT3 is expressed in various tissues, but its expression level is lower than those of OCT1 in the liver and OCT2 in the kidney. The SLC47 family contains two subtypes of H^+/organic cation antiporters called multidrug and toxin extrusion 1 (MATE1/SLC47A1) and kidney-specific MATE2-K (SLC47A2) (Terada and Inui, 2008). Human MATE1 is mostly expressed and located in the luminal side of the renal proximal tubules and bile canaliculi (Otsuka et al., 2005; Masuda et al., 2006) and mediates the secretion of

This work was supported in part by the Ministry of Education, Culture, Sports, Science and Technology of Japan [Grant-in-Aid for Scientific Research].

Article, publication date, and citation information can be found at http://molpharm.aspetjournals.org.

doi:10.1124/mol.109.056242.

ABBREVIATIONS: SLC, solute carrier; MATE, multidrug and toxin extrusion; OCT, organic cation transporter; OCTN, novel organic cation transporter; TEA, tetraethylammonium; kb, kilobase(s); ES, embryonic stem; RT, reverse transcription; PCR, polymerase chain reaction; Gapdh, glyceraldehyde-3-phosphate dehydrogenase; HPLC; high-performance liquid chromatography; CL_{tot}, total body clearance; V_1, central volume of distribution; Q, intercompartmental clearance; Vd_{ss}, volume of distribution at steady state; AUC_{0-60}, area under the blood concentration-time curve from time 0 to 60 min; CL_{ren}, renal clearance; CL_{sec}, renal secretory clearance; Ccr, creatinine clearance; CL_{nr}, nonrenal clearance; $CL_{tissue, r}$, renal tissue clearance; $CL_{tissue, h}$, hepatic tissue clearance; SNP, single nucleotide polymorphism.

organic cations by using an oppositely directed H^+ gradient as a driving force (Tsuda et al., 2009).

In mice, OCT1 and OCT2 are expressed in the basolateral membranes of the kidney (Schweifer and Barlow, 1996; Mooslehner and Allen, 1999) and MATE1 is expressed in the brush-border membranes of the kidney (Otsuka et al., 2005; Hiasa et al., 2006; Kobara et al., 2008). In the liver, OCT1 and MATE1 are expressed in the sinusoidal and canalicular membranes, respectively (Schweifer and Barlow, 1996; Green et al., 1999; Otsuka et al., 2005; Hiasa et al., 2006). MATE2-K has not been identified in rodents.

To elucidate the physiological roles of OCTs, knockout mouse models have been generated for the *Oct1* and *Oct2* genes. *Oct1*(−/−) and *Oct2*(−/−) mice are viable and display no obvious phenotypic abnormalities (Jonker et al., 2001, 2003). However, *Oct1*(−/−) mice showed dramatically reduced hepatic uptake of tetraethylammonium (TEA, a prototypical organic cation) and metformin (Jonker et al., 2001; Wang et al., 2002, 2003). In *Oct1/2* double-knockout mice, the renal secretion of TEA was abolished and the plasma levels of TEA were substantially increased (Jonker et al., 2003). Considering the differences in tissue distribution between mice and humans, a combined deficiency of *Oct1* and *Oct2* better reflects the effect of OCT2 deficiency on the kidney function in humans. These knockout animal studies emphasize the role of OCTs in the hepatic and renal elimination and tissue distribution of cationic drugs. Although information on apical MATE1 obtained in vitro has accumulated, the roles of MATE1 in renal and hepatic function in vivo are still not well understood. In the present study, therefore, we generated *Mate1* knockout mice and demonstrated the physiological and pharmacokinetic significance of MATE1 in vivo.

Materials and Methods

Materials. Metformin hydrochloride was obtained from Sigma-Aldrich Co. (St. Louis, MO). All other chemicals used were of the highest purity available.

Animals. Animal experiments were conducted in accordance with the *Guidelines for Animal Experiments of Kyoto University*. All protocols were approved by the Animal Research Committee, Graduate School of Medicine, Kyoto University. In the present study, male and female mice were mated with each genotype to obtain the adequate sample size. All animals used in the present experiments were male *Mate1*(+/+) (wild-type), *Mate1*(+/−) (heterozygous) or *Mate1*(−/−) (homozygous) mice with the same genetic background (C57BL/6), between 7 and 20 weeks of age. The mice were kept in a temperature-controlled environment with a 12-h light/dark cycle and received a standard diet and water ad libitum.

Construction of the Targeting Vector. Mouse *Mate1* genomic DNA sequences were cloned from a C57BL/6-derived genomic DNA and subcloned into the pPNT vector. A 1.8-kb fragment containing exon 1 was deleted from this construct and replaced with a 1.9-kb fragment with phosphoglycerate kinase 1 promoter and neomycin-resistance gene (*PGKp-neo*^{r}) cassette. A selectable thymidine kinase gene (*tk*) was added at the 3′ arm. The orientation and sequence were verified by restriction analyses.

Generation of Mate1 Knockout Mice. The targeting vector was linearized and electroporated into an embryonic stem (ES) cell line derived from the C57BL/6 mouse strain (Mishina and Sakimura, 2007). Stable clones were selected for resistance to G418. Of 233 G418-resistant clones, six were correctly targeted, as confirmed homologous recombination by Southern blot analysis with 5′, 3′, and neo probes. Hybridization of PvuII-digested genomic DNA with a 5′ probe resulted in a wild-type band of 9.0 kb and a mutated band of 6.4 kb. Hybridization of NcoI-digested genomic DNA with a 3′ probe resulted in a wild-type band of 10.9 kb and a mutated band of 7.8 kb. Blastocysts obtained by aggregation of ICR morula-stage embryos and three different ES cells were transferred to recipient uterus after 3 days of pseudopregnancy. Chimeric male mice were mated with C57BL/6 female mice, and offspring (F1) were genotyped by Southern blot analysis. F2 homozygous mutant mice were then generated by intercrossing F1 heterozygous male and female mice. F2 mice were genotyped by Southern blot analysis of genomic DNA isolated from tail biopsies. In this study, the ES cell line has the pure C57BL/6 genetic background (Mishina and Sakimura, 2007), and therefore we did not perform the back-crossing, which is generally carried out in the generation of knockout mice using 129-derived ES cells and C57BL/6 mice.

Reverse Transcription-Polymerase Chain Reaction and Real-Time PCR. Total RNA was isolated from kidney and liver of mice with the RNeasy Mini Kit (QIAGEN, Hilden, Germany). The total RNA (500 ng) was reverse-transcribed, and the reaction mixtures were used for PCR and real-time PCR. These single-stranded DNA fragments were amplified according to the following profile immediately after an initial 3-min denaturation step at 95°C: 95°C for 30 s, 54°C for 30 s, 72°C for 120 s, 25 cycles for Mate1 in the kidney and glyceraldehyde-3-phosphate dehydrogenase (Gapdh) in the kidney and liver, or 30 cycles for Mate1 in the liver. The specific primer sets for Mate1 and Gapdh are shown in Table 1. The amplified PCR products were separated in a 1% agarose gel and stained with ethidium bromide. Real-time PCR was performed with an ABI PRISM 7700 (Applied Biosystems, Foster City, CA), as described previously (Shimakura et al., 2006). The primer-probe set for mouse Mate2 is summarized in Table 1. The following TaqMan Gene Expression Assays were purchased from Applied Biosystems: Oct1, Mm00456303_m1; Oct2, Mm00457295_m1; Oct3, Mm00488294_m1; Octn1, Mm00457739_m1; Octn2, Mm00441468_m1; Octn3, Mm00490650_m1. Gapdh mRNA was also measured as an internal control with TaqMan Rodent GAPDH Control Reagent (Applied Biosystems).

Western Blot Analysis. Polyclonal antibody was raised against a synthetic peptide corresponding to the intracellular domains of mouse MATE1 (CQQAQVHANLKVN, 466–478) (Masuda et al., 2006). The brush-border membrane fractions from mouse kidneys were prepared the same as brush-border membrane vesicles from rat kidney (Maeda et al., 1993). The membrane fractions were suspended in buffer (100 mM mannitol and 10 mM HEPES-KOH, pH 7.5) and solubilized in NuPAGE LDS sample buffer (Invitrogen, Carlsbad, CA). The samples were separated by SDS-polyacrylamide gel electrophoresis (4–12% NuPAGE Novex Bis-Tris Gel; Invitrogen) and transferred to polyvinylidene difluoride membranes (PVDF

TABLE 1
Primer sets and probe for RT-PCR and real-time PCR
Each position is from the sequence in the GenBank database.

Gene Names (Accession No.)	Position	Sequences (5′ to 3′)
For RT-PCR		
Mouse Mate1 (NM_026183)		
Forward primer	18 to 35	ACGGAGGCCACATGGAAC
Reverse primer	2036 to 2017	TCCACTCCAGAGCATCTCCT
Mouse Gapdh (NM_008084)		
Forward primer	70 to 90	CAGTGCATCTTCTTGTGCAGT
Reverse primer	1238 to 1218	TGTGAGGGAGATGCTCAATGT
For real-time PCR		
Mouse Mate2 (NM_001033542)		
Forward primer	1521 to 1540	TTCGAGCTGGGCTAAAAAGC
Reverse primer	1589 to 1568	CTCTTTCCAAGATGGGCAGATC
TaqMan probe	1542 to 1566	CCAAGGAGTTGATACCCACGCCAGC

membrane 0.2 μm; Invitrogen) using an XCell II Blot Module (Invitrogen) according to the manufacturer's instructions. The blots were blocked with 5% nonfat dry milk in Tris-buffered saline (20 mM Tris and 137 mM NaCl) containing 0.5% Tween 20. The blots were then incubated overnight at 4°C with primary antibody for mouse MATE1 (1:1000 dilution) or villin (1:1000 dilution; Santa Cruz Biotechnology, Inc., Santa Cruz, CA). The bound antibody was detected on X-ray film by enhanced chemiluminescence with horseradish peroxidase-conjugated anti-rabbit IgG (for mouse MATE1) or anti-goat IgG (for villin) antibodies and cyclic diacylhydrazides (GE Healthcare, Chalfont St. Giles, Buckinghamshire, UK). Villin was examined as a positive control.

Histopathological and Blood Biochemical Analyses. Tissues for histopathological analysis were collected from three each of *Mate1*(+/+) and *Mate1*(−/−) mice and processed for hematoxylin and eosin staining. Standard blood biochemical analysis of plasma was performed with a Fuji DRI-CHEM 3500V (Fujifilm Medical Co., Ltd., Tokyo, Japan).

Pharmacokinetic Experiments. Mice were anesthetized with an intraperitoneal administration of 50 mg/kg sodium pentobarbital. A catheter was inserted into the right jugular vein with polyethylene tubing (Intramedic PE-10; BD Biosciences, San Jose, CA) for drug administration. Urine was collected from the urinary bladder catheterized with SP-31 tubing (Natsume Seisakusho, Tokyo, Japan). Thereafter, 5 mg/kg metformin and 146 mg/kg mannitol were administered as a bolus via the jugular vein. Then, 1% mannitol was administered to maintain a sufficient and constant urine flow rate by continuous infusion at 0.35 ml/h using an automatic infusion pump (Harvard Apparatus, Inc., Holliston, MA). Blood samples were collected from both femoral veins at 1, 5, 15, and 30 min and from the abdominal aorta at 60 min after drug administration. Urine was collected for 60 min after drug administration. At the end of the experiment, the kidney and liver were removed to determine the tissue concentration of metformin. The concentrations of metformin in plasma, urine, the renal homogenate, and the hepatic homogenate were determined by high-performance liquid chromatography (HPLC) (Kimura et al., 2005). The plasma samples were obtained by centrifugation of blood. Plasma or urine (25 μl) was deproteinized by adding 50 μl of methanol. The samples were centrifuged and supernatants from plasma or urine were diluted 4- or 200-fold with saline, respectively. The supernatants were filtered through a filter (SGJVL; 0.45 μm; Millipore, Billerica, MA) and injected (50 μl) into the HPLC system. The excised tissues were gently washed, weighed, and homogenized in 9 volumes of saline. Homogenates (150 μl) were deproteinized by adding 300 μl of methanol, and the samples were centrifuged. The supernatants were filtered through a Millipore filter (SGJVL, 0.45 μm) and injected (50 μl) into the HPLC system. The levels of creatinine in plasma and urine at 60 min were determined with the Jaffé reaction with an assay kit from Wako Pure Chemical Industries (Osaka, Japan).

Determination of Pharmacokinetic Parameters. A conventional two-compartmental analysis was used to investigate the plasma concentration-time profiles of metformin after the intravenous administration in mice using WinNonlin version 5.2.1 (Pharsight Corporation, Mountain View, CA). Pharmacokinetic parameters, the area under the blood concentration-time curve from time 0 to infinity (AUC_{∞}), total body clearance (CL_{tot}), central volume of distribution (V_1), intercompartmental clearance (Q), and volume of distribution at steady state (Vd_{ss}), were calculated by the nonlinear least-squares method. The AUC until 60 min (AUC_{0-60}) was deter-

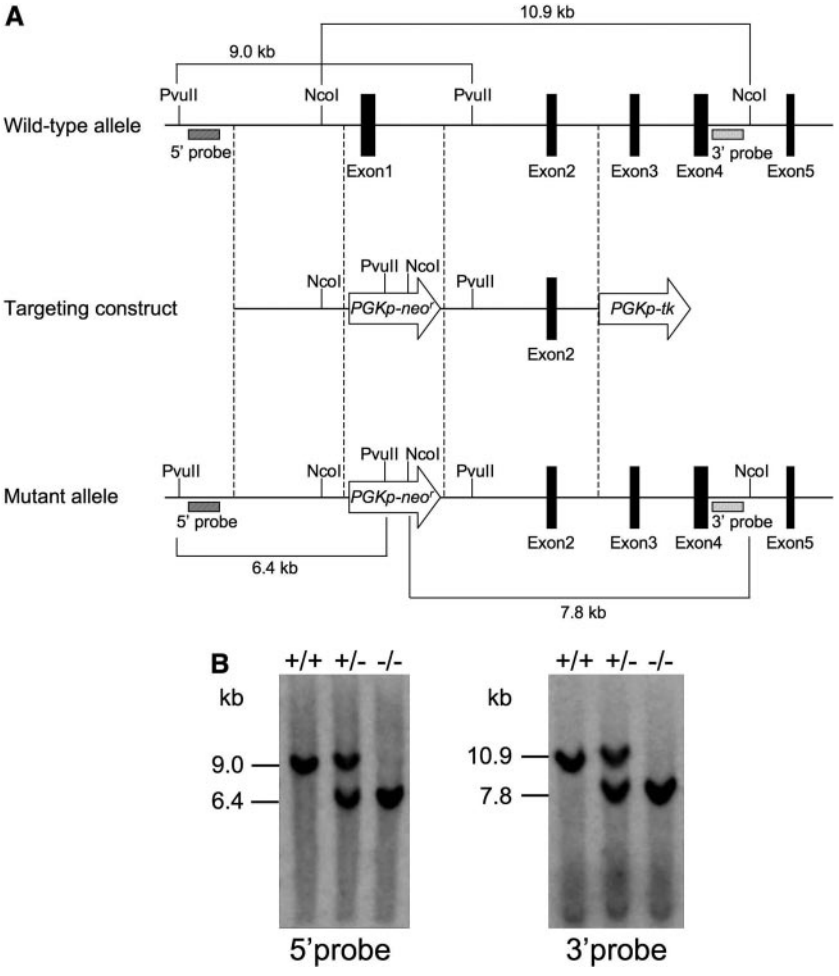

Fig. 1. Targeted disruption of the mouse *Mate1* gene by homologous recombination. A, in the diagrams of the wild-type and mutant alleles, exons are indicated by closed boxes. In the targeting construct, exon 1 was replaced with a *PGKp-neo*^{r} cassette. Only relevant restriction sites are indicated. For Southern blot analysis, 5′ and 3′ probes were used on PvuII- and NcoI-digested genomic DNA, respectively. Sizes of diagnostic restriction fragments for wild-type and targeted alleles are indicated. B, Southern blot analysis of genomic DNA from mouse tail biopsy samples by digestion with PvuII and hybridization with the 5′ probe (left) and with NcoI and hybridization with the 3′ probe (right).

mined by the trapezoidal rule. Renal clearance (CL_{ren}) of metformin was obtained by dividing the amounts of metformin eliminated into urine during 60 min by the AUC_{0-60}. The renal secretory clearance (CL_{sec}) of metformin was calculated by subtracting creatinine clearance (Ccr) from CL_{ren}, assuming that the protein binding of metformin in plasma is negligible (Sirtori et al., 1978; Pentikäinen et al., 1979). The nonrenal clearance (CL_{nr}) of metformin was calculated by subtracting CL_{ren} from CL_{tot}. The renal tissue clearance ($CL_{tissue,\ r}$) and hepatic tissue clearance ($CL_{tissue,\ h}$) of metformin were calculated by dividing the tissue accumulation of metformin at 60 min by the AUC_{0-60}.

Statistical Analysis. All data were expressed as the mean ± S.D. Data from real-time PCR were analyzed statistically with the one-way analysis of variance followed by Dunnett's test. Data from blood biochemical analysis and pharmacokinetic analysis were analyzed statistically using the unpaired *t* test.

Results

Targeted Disruption of the *Mate1* Gene. The mouse *Mate1* gene was disrupted by replacing the coding region of exon 1 with a *PGKp-neo*^{r} cassette via homologous recombination in ES cells (Fig. 1A). Correct targeting of the *Mate1* locus in ES cell clones was determined by Southern blot analysis (data not shown). Chimeric mice were generated from ES cells and mated with C57BL/6 mice, resulting in germ line transmission, which was proven by Southern blot analysis (data not shown). Heterozygous male and female mice were mated to produce wild-type and *Mate1* knockout mice. The targeted *Mate1* allele was detected in these offspring by Southern blot analysis of genomic DNA isolated from tail biopsies (Fig. 1B).

Analyses of Mate1 mRNA and MATE1 Protein Expression. To verify that the targeting event resulted in a *Mate1* null mutation, the lack of expression of Mate1 mRNA and MATE1 protein was determined. No Mate1 mRNA expression was detected in the kidney (Fig. 2A) and liver (Fig. 2B) of *Mate1*(−/−) mice by RT-PCR. Western blot analysis demonstrated that MATE1 protein was undetectable in renal brush-border membranes of *Mate1*(−/−) mice (Fig. 2C).

Analyses of mRNA Expression of Organic Cation Transporters. To clarify whether mRNA levels of other organic cation transporters are changed in *Mate1*(−/−) mice, the mRNA expression of seven organic cation transporters in the kidney and liver was investigated by real-time PCR. As shown in Fig. 3A, no differences in mRNA levels of Oct1, Oct2, Octn1 and Octn2 in the kidney were observed among *Mate1*(+/+), *Mate1*(+/−), and *Mate1*(−/−) mice. Mate2, Oct3, and Octn3 mRNA expression was little observed in the kidney. In the liver, no differences in the expression of Oct1 and Octn2 mRNA were observed among *Mate1*(+/+), *Mate1*(+/−), and *Mate1*(−/−) mice (Fig. 3B). Mate2, Oct2, Oct3, Octn1, and Octn3 mRNA expression was little observed in the liver.

Initial Phenotypic Analyses. *Mate1*(−/−) mice were found to be viable, fertile and of normal body weight. Histopathological examinations excluded any genotype-related abnormalities in 18 tissues (adrenal, bladder, cerebellum, cerebrum, duodenum, esophagus, heart, ileum, jejunum, kidney, liver, pancreas, pituitary gland, spleen, stomach, testis, thyroid, and trachea; data not shown). Blood biochemical analyses revealed significant elevations of plasma creatinine and blood urea nitrogen (BUN) levels in *Mate1*(−/−) mice. Other parameters showed no significant changes between *Mate1*(+/+) and *Mate1*(−/−) mice (Table 2).

Pharmacokinetics of Metformin in *Mate1*(+/+) *and Mate1*(−/−) Mice. We then compared pharmacokinetic profiles of metformin, a typical substrate of MATE1, in *Mate1*(+/+) and *Mate1*(−/−) mice. The plasma concentration of metformin was markedly elevated in *Mate1*(−/−) mice compared with *Mate1*(+/+) mice (Fig. 4). Furthermore, urinary excretion of metformin for 60 min after the intravenous administration was significantly decreased in *Mate1*(−/−) mice (Fig. 5). Table 3 summarizes the pharmacokinetic parameters of metformin in *Mate1*(+/+) and *Mate1*(−/−) mice. The AUC_{0-60} for metformin in *Mate1*(−/−) mice was 2-fold higher than that in *Mate1*(+/+) mice. The CL_{tot} of metformin was significantly decreased in *Mate1*(−/−) mice compared with *Mate1*(+/+) mice. The CL_{ren} of metformin in *Mate1*(−/−) mice was approximately 18% of that in

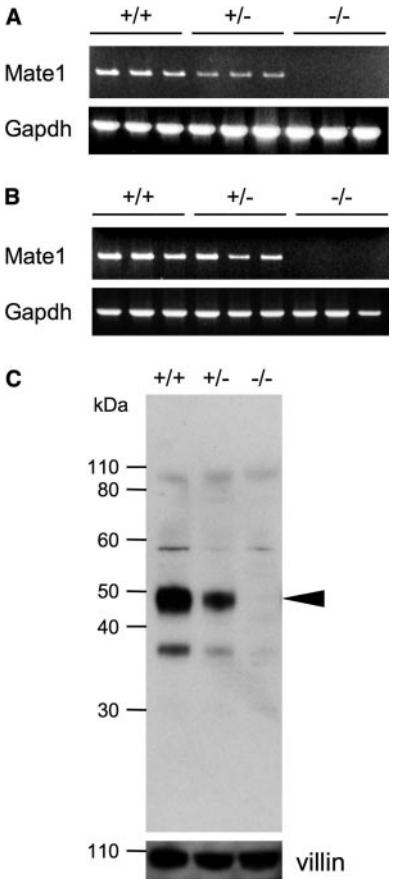

Fig. 2. Mate1 mRNA and MATE1 protein expression in *Mate1*(+/+), *Mate1*(+/−), and *Mate1*(−/−) mice. RT-PCR analyses for mouse Mate1 in the kidney (A) and liver (B). Total RNA isolated from mice kidney and liver was reverse-transcribed, and the synthesized cDNA was amplified using a set of specific primers for Mate1 or Gapdh. The PCR products of 2019 bp that corresponded to Mate1 were separated by 1% agarose gel electrophoresis, and stained with ethidium bromide. The quality of the sample RNA was also checked by RT-PCR for Gapdh as an internal control. C, Western blot analysis of MATE1 in renal brush-border membranes of *Mate1*(+/+), *Mate1*(+/−), and *Mate1*(−/−) mice. Renal brush-border membranes (20 μg) were separated by SDS-polyacrylamide gel electrophoresis (4–12%) and blotted onto polyvinylidene difluoride membranes. The antiserum for mouse MATE1 (1:1000) was used as a primary antibody. A horseradish peroxidase-conjugated anti-rabbit IgG antibody was used for detection of bound antibodies, and the strips of blots were visualized by chemiluminescence on X-ray film. The arrowhead indicates the position of mouse MATE1.

Mate1(+/+) mice, whereas the CL_{nr} was not significantly changed. There were modest differences in Ccr between *Mate1*(+/+) and *Mate1*(−/−) mice. The CL_{sec} of metformin in *Mate1*(−/−) mice was approximately 14% of that in *Mate1*(+/+) mice. The Q, V_1, and Vd_{ss} of metformin were not changed between *Mate1*(+/+) and *Mate1*(−/−) mice.

Figure 6, A and B, shows the renal and hepatic concentrations of metformin in *Mate1*(+/+) and *Mate1*(−/−) mice at 60 min after the intravenous administration of metformin. The metformin concentrations in the kidney and liver were significantly elevated in *Mate1*(−/−) mice compared with *Mate1*(+/+) mice. To correct the tissue concentrations by plasma concentration, tissue clearance was determined by dividing the tissue concentration of metformin at 60 min by the AUC_{0-60}. As shown in Fig. 6, C and D, $CL_{tissue,\,r}$ and $CL_{tissue,\,h}$ of metformin were also significantly increased in *Mate1*(−/−) mice.

Discussion

Previous studies using renal brush-border membrane vesicles, cultured renal cell lines, and heterologous expression systems of MATE1 provided indirect evidences for pharmacokinetic importance of H^+/organic cation antiporters for renal secretion process of organic cations. The present pharmacokinetic analysis revealed that plasma and renal concentration of metformin were markedly elevated in *Mate1*(−/−) mice compared with *Mate1*(+/+) mice (Figs. 4 and 6A). Urinary excretion of metformin for 60 min after the intravenous administration was significantly decreased in *Mate1*(−/−) mice (33% of dose) compared with *Mate1*(+/+) mice (79% of dose) (Fig. 5). The $CL_{tissue,\,r}$ of metformin was also signifi-

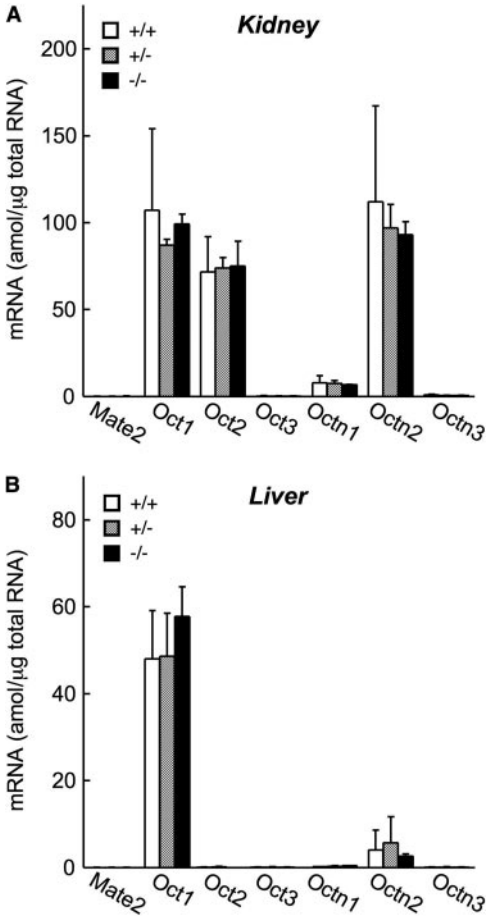

Fig. 3. Organic cation transporters mRNA expression in the kidney (A) and liver (B). Total RNA isolated from the kidney and liver of *Mate1*(+/+) (□), *Mate1*(+/−) (▨), and *Mate1*(−/−) (■) mice was reverse-transcribed and mRNA levels of seven organic cation transporters were determined by real-time PCR with the oligonucleotides summarized in Table 1 and under *Materials and Methods* using an ABI PRISM 7700 sequence detector. The results corrected by Gapdh levels are mean ± S.D. for three mice among each genotype.

TABLE 2

Blood biochemical parameters of *Mate1*(+/+) and *Mate1*(−/−) mice

Each value represents the mean ± S.D. for six mice.

Parameter	+/+	−/−
Total protein (g/dl)	3.9 ± 0.1	3.3 ± 0.6
Albumin (g/dl)	2.0 ± 0.1	1.7 ± 0.3
Creatinine (mg/dl)	0.1 ± 0.0	0.3 ± 0.1***
BUN (mg/dl)	26.1 ± 0.8	30.5 ± 1.6***
Uric acid (mg/dl)	0.6 ± 0.4	0.6 ± 0.3
Glucose (mg/dl)	253 ± 29	254 ± 20
Total cholesterol (mg/dl)	58 ± 3	66 ± 11
Triglyceride (mg/dl)	87 ± 29	98 ± 19
HDL (mg/dl)	46 ± 7	47 ± 7
Sodium (mEq/l)	140 ± 7	133 ± 22
Potassium (mEq/l)	4.0 ± 0.5	3.8 ± 0.7
Chloride (mEq/l)	106 ± 6	99 ± 18
Phosphorus (mg/dl)	7.8 ± 0.6	8.3 ± 1.2
Magnesium (mg/dl)	1.9 ± 0.3	2.0 ± 0.2
ALP (U/l)	486 ± 67	466 ± 52
CPK (U/l)	67 ± 14	70 ± 9
AST (U/l)	33 ± 4	36 ± 8
ALT (U/l)	25 ± 4	27 ± 6
γ-GTP (U/l)	3 ± 1	4 ± 1
LAP (U/l)	39 ± 3	40 ± 2
Amylase (U/l)	2812 ± 645	2884 ± 553
LDH (U/l)	246 ± 72	221 ± 24
Total bilirubin (mg/dl)	0.3 ± 0.1	0.3 ± 0.1

BUN, blood urea nitrogen; HDL, high-density lipoprotein; ALP, alkaline phosphatase; CPK, creatine kinase; AST, aspartate aminotransferase; ALT, alanine aminotransferase; γ-GTP, γ-glutamyltranspeptidase; LAP, leucine aminopeptidase; LDH, lactate dehydrogenase.

*** $P < 0.001$, significantly different from *Mate1*(+/+) mice.

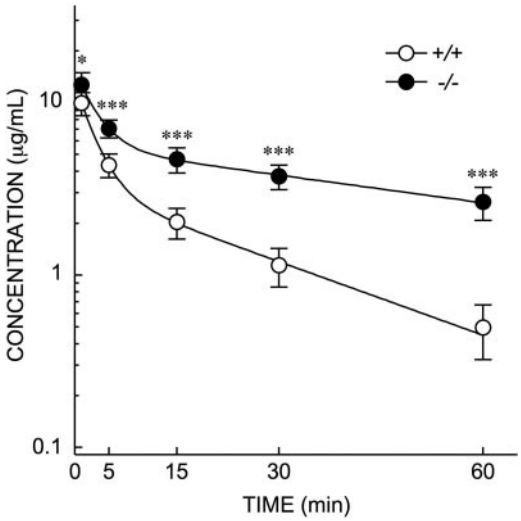

Fig. 4. Plasma concentration profile of metformin in *Mate1*(+/+) (○) and *Mate1*(−/−) (●) mice. Metformin at 5 mg/kg and mannitol at 146 mg/kg were administered as a bolus via the jugular vein. Then, 1% mannitol was administered to maintain a sufficient and constant urine flow rate by continuous infusion at 0.35 ml/h using an automatic infusion pump. Thereafter, blood samples were collected at the time points indicated. Metformin levels in the blood samples were determined by HPLC. Each point represents the mean ± S.D. for six mice of each genotype. *, $P < 0.05$; ***, $P < 0.001$, significantly different from *Mate1*(+/+) mice.

cantly increased in *Mate1*(−/−) mice (Fig. 6C), although mRNA levels of Oct1 and Oct2, transporting metformin from blood into the cells, in the kidney were not changed between *Mate1*(+/+) and *Mate1*(−/−) mice (Fig. 3A). Furthermore, as shown in Table 3, pharmacokinetic analysis demonstrated the significant decrease of the CL_{tot}, CL_{ren}, and CL_{sec} of metformin in *Mate1*(−/−) mice, whereas the CL_{nr}, Q, V_1, and Vd_{ss} were little affected by the lack of MATE1 protein. Taken together, in the present study, we determined for the first time that MATE1 plays crucial roles in the renal secretion process of metformin in vivo.

It has been reported that the lack of OCT1 protein did not affect the plasma concentration of metformin, but the hepatic concentration of metformin was significantly reduced in *Oct1*(−/−) mice (Wang et al., 2002, 2003; Shu et al., 2007). A decrease of the hepatic uptake of metformin caused a reduction in the effect of metformin on AMP-activated protein kinase phosphorylation and gluconeogenesis, and the glucose-lowering effects of metformin were completely abolished (Shu et al., 2007). These findings suggested that the lack of transport activity of OCT1 affects not only the pharmacokinetics but also the therapeutic actions of cationic drugs. Regarding the *Mate1*(−/−) mice, the concentration of metformin was elevated in the liver (Fig. 6B), suggesting that *Mate1*(−/−) mice may cause greater glucose-lowering effects of metformin than *Mate1*(+/+) mice. Our group recently identified five nonsynonymous coding single nucleotide polymorphisms (SNPs) encoding MATE1 (V10L, G64D, A310V, D328A, and N474S) and an SNP in the promoter region of *MATE1* gene (−32G>A) that affects the promoter activity (Kajiwara et al., 2007, 2009). In their coding SNPs, the three variants (G64D, A310V, and D328A) showed significantly decreased in the transport activity of metformin. Another group also identified six nonsynonymous coding SNPs encoding MATE1 (Chen et al., 2009). Furthermore, it was reported that the rs2289669G>A SNP located in an intron of *MATE1* gene is associated with a reduction in HbA1c level in patients with diabetes mellitus who received metformin therapy, suggesting that MATE1 may have an important role in the pharmacokinetics and pharmacodynamics of metformin (Becker et al., 2009). By using *Mate1*(−/−) mice, the relationship between the pharmacological effects of metformin and the transport activity of MATE1 would be clarified.

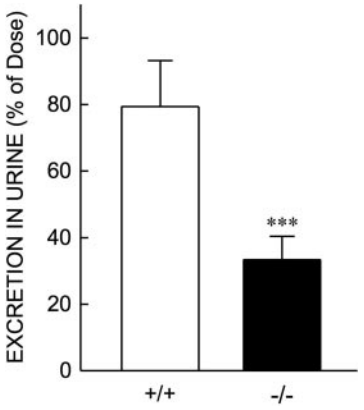

Fig. 5. Urinary excretion of metformin in *Mate1*(+/+) (open column) and *Mate1*(−/−) (closed column) mice. Metformin and mannitol administration was carried out as described in Fig. 4. Urine was collected for 60 min after the drug administration. Metformin levels in the urine samples were determined by HPLC. Each column represents the mean ± S.D. for six mice. ***, $P < 0.001$, significantly different from *Mate1*(+/+) mice.

TABLE 3

Pharmacokinetic parameters of metformin and Ccr in *Mate1*(+/+) and *Mate1*(−/−) mice

The CL_{ren} of metformin was obtained by dividing the amounts of metformin eliminated into urine during 60 min by the AUC_{0-60}. The CL_{sec} of metformin was calculated by subtracting Ccr from CL_{ren}, assuming that the protein binding of metformin in plasma is negligible. The CL_{nr} of metformin was calculated by subtracting CL_{ren} from CL_{tot}. Each value represents the mean ± S.D. for six mice.

Parameter	+/+	−/−
AUC_{0-60} (μg · min/ml)	108.7 ± 17.0	257.2 ± 39.6***
AUC_{∞} (μg · min/ml)	126.3 ± 23.3	525.7 ± 152.4**
CL_{tot} (mL/min/kg)	40.7 ± 7.0	10.2 ± 2.7***
CL_{ren} (mL/min/kg)	37.2 ± 8.5	6.6 ± 1.3***
CL_{nr} (mL/min/kg)	3.5 ± 5.3	3.6 ± 2.0
CL_{sec} (mL/min/kg)	31.8 ± 7.3	4.3 ± 1.2***
Q (mL/min/kg)	70.6 ± 22.5	59.5 ± 9.1
V_1 (mL/kg)	392 ± 62	334 ± 88
Vd_{ss} (mL/kg)	994 ± 192	853 ± 245
Ccr (mL/min/kg)	5.4 ± 2.9	2.2 ± 0.8*

* $P < 0.05$, significantly different from *Mate1*(+/+) mice.
** $P < 0.01$, significantly different from *Mate1*(+/+) mice.
*** $P < 0.001$, significantly different from *Mate1*(+/+) mice.

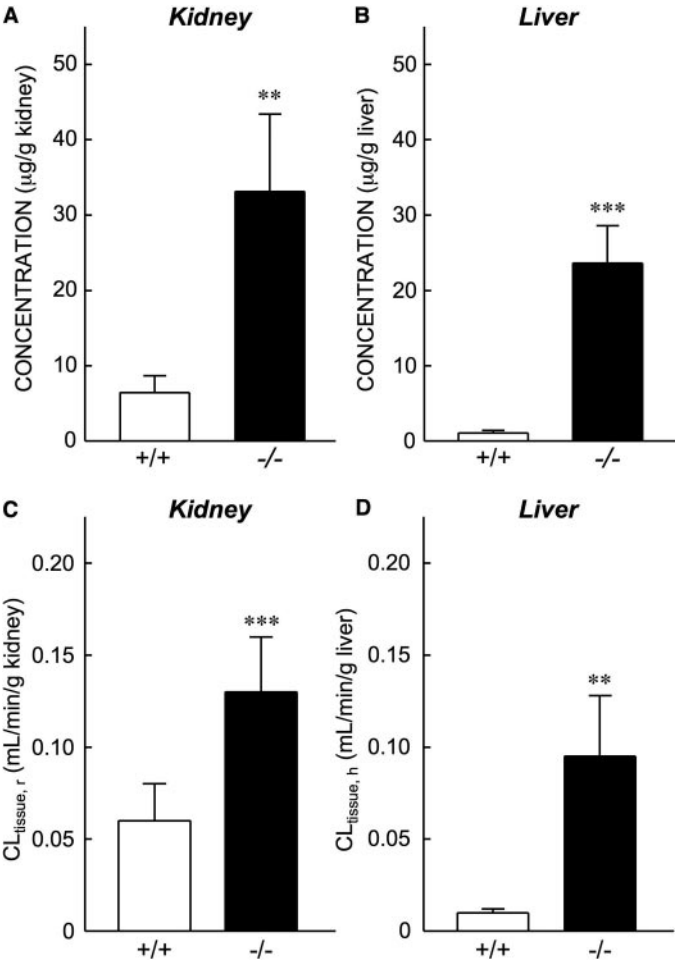

Fig. 6. Tissue distribution (A, B) and tissue clearance (C, D) of metformin in *Mate1*(+/+) (□) and *Mate1*(−/−) (■) mice. Metformin and mannitol administration was carried out as described in Fig. 4. The kidney (A and C) and liver (B and D) were removed to determine the tissue concentration of metformin at 60 min after the drug administration. Metformin levels in the tissue samples were determined by HPLC. The $CL_{tissue, r}$ and $CL_{tissue, h}$ of metformin were calculated by dividing the tissue accumulation at 60 min by the AUC_{0-60}. Each column represents the mean ± S.D. for six mice. **, $P < 0.01$; ***, $P < 0.001$, significantly different from *Mate1*(+/+) mice.

In this study, *Mate1*(−/−) mice were found to be viable, fertile, and of normal body weight. Furthermore, no histopathological differences were observed between *Mate1*(+/+) and *Mate1*(−/−) mice. On the other hand, blood biochemical analysis revealed significant elevations of plasma creatinine and BUN levels in *Mate1*(−/−) mice (Table 2). In the pharmacokinetic study, the Ccr of *Mate1*(−/−) mice was mildly decreased compared with that of *Mate1*(+/+) mice (Table 3). These data may indicate that mild nephropathy occurred in the *Mate1*(−/−) mice. Long-term follow-up under various conditions could clarify the influence of the lack of MATE1 protein on the renal function.

It has been reported that the expression levels of multidrug resistance protein 4 (Mrp4/Abcc4) mRNA and protein in the kidney were increased in *Mrp2* (*Abcc2*) knockout mice (Chu et al., 2006; Vlaming et al., 2006). The induction of Mrp4 expression has been considered a compensatory mechanism induced by the absence of *Mrp2* because MRP2 and MRP4 have similar substrate specificity. In the present study, the clear compensatory regulation of other organic cation transporters was not observed in the kidney and liver (Fig. 3, A and B). These results suggest that *Mate1*(−/−) mice are an appropriate model for characterizing the pharmacokinetic roles of MATE1 in vivo because expression levels of other organic cation transporters with similar substrate specificity to MATE1 were not changed.

There are two mouse MATE1 variants, MATE1a and MATE1b (Otsuka et al., 2005; Hiasa et al., 2006; Kobara et al., 2008), consisting of 532 and 567 amino acid residues, respectively. Mammalian MATE transporters commonly possess a long hydrophobic tail at the carboxyl terminal (Otsuka et al., 2005; Ohta et al., 2006; Terada et al., 2006; Zhang et al., 2007), but MATE1a is an exception and lacks such a sequence. On the other hand, MATE1b has almost the same carboxyl terminal amino acid sequence as the human, rat and rabbit MATE1 proteins, and has been considered the true counterpart of the MATE1 group. In the present study, we generated *Mate1* knockout mice, disrupting the *Mate1* gene by replacing the coding region of the first exon with a *PGKp-neo*^{r} cassette. Therefore, a complete absence of MATE1a and MATE1b proteins is expected in *Mate1* knockout mice. Western blot analysis using MATE1 antibody, which can recognize both MATE1a and MATE1b proteins, demonstrated that MATE1 protein was undetectable in the kidney of *Mate1*(−/−) mice (Fig. 2C).

In conclusion, we generated *Mate1* knockout mice for the first time and demonstrated that this transporter plays crucial roles in the renal clearance of metformin, a typical substrate of MATE1. These results suggest that MATE1 plays an important role in the secretion of organic cations from the kidney.

References

Becker ML, Visser LE, van Schaik RH, Hofman A, Uitterlinden AG, and Stricker BH (2009) Genetic variation in the multidrug and toxin extrusion 1 transporter protein influences the glucose-lowering effect of metformin in patients with diabetes: a preliminary study. *Diabetes* **58:**745–749.

Chen Y, Teranishi K, Li S, Yee SW, Hesselson S, Stryke D, Johns SJ, Ferrin TE, Kwok P, and Giacomini KM (2009) Genetic variants in multidrug and toxic compound extrusion-1, hMATE1, alter transport function. *Pharmacogenomics J* **9:**127–136.

Chu XY, Strauss JR, Mariano MA, Li J, Newton DJ, Cai X, Wang RW, Yabut J, Hartley DP, Evans DC, et al. (2006) Characterization of mice lacking the multidrug resistance protein Mrp2 (Abcc2). *J Pharmacol Exp Ther* **317:**579–589.

Green RM, Lo K, Sterritt C, and Beier DR (1999) Cloning and functional expression of a mouse liver organic cation transporter. *Hepatology* **29:**1556–1562.

Hiasa M, Matsumoto T, Komatsu T, and Moriyama Y (2006) Wide variety of locations for rodent MATE1, a transporter protein that mediates the final excretion step for toxic organic cations. *Am J Physiol Cell Physiol* **291:**C678–C686.

Inui K, Masuda S, and Saito H (2000) Cellular and molecular aspects of drug transport in the kidney. *Kidney Int* **58:**944–958.

Jonker JW, Wagenaar E, Mol CA, Buitelaar M, Koepsell H, Smit JW, and Schinkel AH (2001) Reduced hepatic uptake and intestinal excretion of organic cations in mice with a targeted disruption of the organic cation transporter 1 (*Oct1* [*Slc22a1*]) gene. *Mol Cell Biol* **21:**5471–5477.

Jonker JW, Wagenaar E, Van Eijl S, and Schinkel AH (2003) Deficiency in the organic cation transporters 1 and 2 (Oct1/Oct2 [Slc22a1/Slc22a2]) in mice abolishes renal secretion of organic cations. *Mol Cell Biol* **23:**7902–7908.

Kajiwara M, Terada T, Asaka J, Ogasawara K, Katsura T, Ogawa O, Fukatsu A, Doi T, and Inui K (2007) Critical roles of Sp1 in gene expression of human and rat H^+/organic cation antiporter MATE1. *Am J Physiol Renal Physiol* **293:**F1564–F1570.

Kajiwara M, Terada T, Ogasawara K, Iwano J, Katsura T, Fukatsu A, Doi T, and Inui K (2009) Identification of multidrug and toxin extrusion (MATE1 and MATE2-K) variants with complete loss of transport activity. *J Hum Genet* **54:**40–46.

Kimura N, Masuda S, Tanihara Y, Ueo H, Okuda M, Katsura T, and Inui K (2005) Metformin is a superior substrate for renal organic cation transporter OCT2 rather than hepatic OCT1. *Drug Metab Pharmacokinet* **20:**379–386.

Kobara A, Hiasa M, Matsumoto T, Otsuka M, Omote H, and Moriyama Y (2008) A novel variant of mouse MATE-1 H^+/organic cation antiporter with a long hydrophobic tail. *Arch Biochem Biophys* **469:**195–199.

Koepsell H, Lips K, and Volk C (2007) Polyspecific organic cation transporters: structure, function, physiological roles, and biopharmaceutical implications. *Pharm Res* **24:**1227–1251.

Maeda S, Takano M, Okano T, Ohoka K, Inui K, and Hori R (1993) Transport of organic cation in renal brush-border membrane from rats with renal ischemic injury. *Biochim Biophys Acta* **1150:**103–110.

Masuda S, Terada T, Yonezawa A, Tanihara Y, Kishimoto K, Katsura T, Ogawa O, and Inui K (2006) Identification and functional characterization of a new human kidney-specific H^+/organic cation antiporter, kidney-specific multidrug and toxin extrusion 2. *J Am Soc Nephrol* **17:**2127–2135.

Mishina M and Sakimura K (2007) Conditional gene targeting on the pure C57BL/6 genetic background. *Neurosci Res* **58:**105–112.

Mooslehner KA and Allen ND (1999) Cloning of the mouse organic cation transporter 2 gene, *Slc22a2*, from an enhancer-trap transgene integration locus. *Mamm Genome* **10:**218–224.

Ohta KY, Inoue K, Hayashi Y, and Yuasa H (2006) Molecular identification and functional characterization of rat multidrug and toxin extrusion type transporter 1 as an organic cation/H^+ antiporter in the kidney. *Drug Metab Dispos* **34:**1868–1874.

Otsuka M, Matsumoto T, Morimoto R, Arioka S, Omote H, and Moriyama Y (2005) A human transporter protein that mediates the final excretion step for toxic organic cations. *Proc Natl Acad Sci U S A* **102:**17923–17928.

Pentikäinen PJ, Neuvonen PJ, and Penttilä A (1979) Pharmacokinetics of metformin after intravenous and oral administration to man. *Eur J Clin Pharmacol* **16:**195–202.

Schweifer N and Barlow DP (1996) The *Lx1* gene maps to mouse chromosome 17 and codes for a protein that is homologous to glucose and polyspecific transmembrane transporters. *Mamm Genome* **7:**735–740.

Shimakura J, Terada T, Saito H, Katsura T, and Inui K (2006) Induction of intestinal peptide transporter 1 expression during fasting is mediated via peroxisome proliferator-activated receptor alpha. *Am J Physiol Gastrointest Liver Physiol* **291:**G851–G856.

Shu Y, Sheardown SA, Brown C, Owen RP, Zhang S, Castro RA, Ianculescu AG, Yue L, Lo JC, Burchard EG, et al. (2007) Effect of genetic variation in the organic cation transporter 1 (OCT1) on metformin action. *J Clin Invest* **117:**1422–1431.

Sirtori CR, Franceschini G, Galli-Kienle M, Cighetti G, Galli G, Bondioli A, and Conti F (1978) Disposition of metformin (N,N-dimethylbiguanide) in man. *Clin Pharmacol Ther* **24:**683–693.

Terada T and Inui K (2008) Physiological and pharmacokinetic roles of H^+/organic cation antiporters (MATE/SLC47A). *Biochem Pharmacol* **75:**1689–1696.

Terada T, Masuda S, Asaka J, Tsuda M, Katsura T, and Inui K (2006) Molecular cloning, functional characterization and tissue distribution of rat H^+/organic cation antiporter MATE1. *Pharm Res* **23:**1696–1701.

Tsuda M, Terada T, Ueba M, Sato T, Masuda S, Katsura T and Inui K (2009) Involvement of human multidrug and toxin extrusion 1 in the drug interaction between cimetidine and metformin in renal epithelial cells. *J Pharmacol Exp Ther* **329:**185–191.

Vlaming ML, Mohrmann K, Wagenaar E, de Waart DR, Elferink RP, Lagas JS, van Tellingen O, Vainchtein LD, Rosing H, Beijnen JH, et al. (2006) Carcinogen and anticancer drug transport by Mrp2 in vivo: studies using *Mrp2* (*Abcc2*) knockout mice. *J Pharmacol Exp Ther* **318:**319–327.

Wang DS, Jonker JW, Kato Y, Kusuhara H, Schinkel AH, and Sugiyama Y (2002) Involvement of organic cation transporter 1 in hepatic and intestinal distribution of metformin. *J Pharmacol Exp Ther* **302:**510–515.

Wang DS, Kusuhara H, Kato Y, Jonker JW, Schinkel AH, and Sugiyama Y (2003) Involvement of organic cation transporter 1 in the lactic acidosis caused by metformin. *Mol Pharmacol* **63:**844–848.

Zhang X, Cherrington NJ, and Wright SH (2007) Molecular identification and functional characterization of rabbit MATE1 and MATE2-K. *Am J Physiol Renal Physiol* **293:**F360–F370.

Address correspondence to: Professor Ken-ichi Inui, Ph.D., Department of Pharmacy, Kyoto University Hospital, Sakyo-ku, Kyoto 606-8507, Japan. E-mail: inui@kuhp.kyoto-u.ac.jp